

This is a repository copy of *Efficient Silicon Metasurfaces for Visible Light*.

White Rose Research Online URL for this paper:

<https://eprints.whiterose.ac.uk/118859/>

Version: Accepted Version

---

**Article:**

Zhou, Zhenpeng, Li, Juntao, Su, Rongbin et al. (9 more authors) (2017) Efficient Silicon Metasurfaces for Visible Light. ACS Photonics. pp. 544-551. ISSN 2330-4022

<https://doi.org/10.1021/acsphotonics.6b00740>

---

**Reuse**

Items deposited in White Rose Research Online are protected by copyright, with all rights reserved unless indicated otherwise. They may be downloaded and/or printed for private study, or other acts as permitted by national copyright laws. The publisher or other rights holders may allow further reproduction and re-use of the full text version. This is indicated by the licence information on the White Rose Research Online record for the item.

**Takedown**

If you consider content in White Rose Research Online to be in breach of UK law, please notify us by emailing [eprints@whiterose.ac.uk](mailto:eprints@whiterose.ac.uk) including the URL of the record and the reason for the withdrawal request.

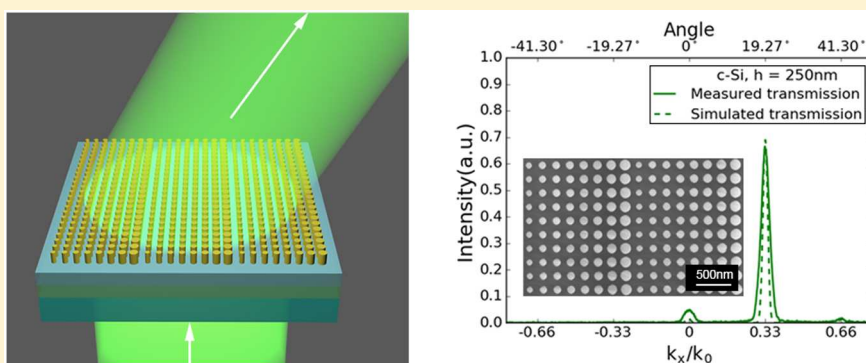
# Efficient Silicon Metasurfaces for Visible Light

Zhenpeng Zhou,<sup>†,‡,||</sup> Juntao Li,<sup>†,‡,||</sup> Rongbin Su,<sup>†,‡</sup> Beimeng Yao,<sup>†,‡</sup> Hanlin Fang,<sup>†,‡</sup> Kezheng Li,<sup>†,‡</sup> Lidan Zhou,<sup>†</sup> Jin Liu,<sup>†,‡</sup> Daan Stellinga,<sup>§</sup> Christopher P. Reardon,<sup>§</sup> Thomas F. Krauss,<sup>†,§</sup> and Xuehua Wang<sup>\*,†,‡</sup>

<sup>†</sup>State Key Laboratory of Optoelectronic Materials and Technologies and <sup>‡</sup>School of Physics, Sun Yat-Sen University, Guangzhou, 510275, China

<sup>§</sup>Department of Physics, University of York, York, YO10 SDD, U.K.

**S** Supporting Information



**ABSTRACT:** Dielectric metasurfaces require high refractive index contrast materials for optimum performance. This requirement imposes a severe restraint; either devices have been demonstrated at wavelengths of 700 nm and above using high-index semiconductors such as silicon, or they use lower index dielectric materials such as TiO<sub>2</sub> or Si<sub>3</sub>N<sub>4</sub> and operate in the visible wavelength regime. Here, we show that the high refractive index of silicon can be exploited at wavelengths as short as 532 nm by demonstrating a crystalline silicon metasurface with a transmission efficiency of 71% at this wavelength and a diffraction efficiency of 95% into the desired diffraction order. The metasurfaces consist of a graded array of silicon posts arranged in a square lattice on a quartz substrate. We show full  $2\pi$  phase control, and we experimentally demonstrate polarization-independent beam deflection at 532 nm wavelength. Our results open a new way for realizing efficient metasurfaces based on silicon for the technologically all-important display applications.

**KEYWORDS:** dielectric metasurfaces, crystalline silicon, wavefront control, diffractive optics

Metasurfaces are ultrathin optical elements that can manipulate optical wavefronts by modifying the phase, amplitude, or polarization of light waves on a subwavelength scale.<sup>1–6</sup> Metasurfaces offer new degrees of freedom for controlling light beams on a smaller scale and with higher accuracy than is possible with conventional bulky optical components. Initial demonstrations of metasurfaces involved plasmonic resonances, which, however, are rather lossy and exhibit low efficiency.<sup>7,8</sup> More recently, all-dielectric metasurfaces have come to the fore because of their high transmission.<sup>9–11</sup> Compared to plasmonic metasurfaces, they offer lower loss, yet they still exhibit Mie resonances for both polarizations at optical frequencies, which has been used to realize perfect reflectors,<sup>12</sup> magnetic mirrors,<sup>13</sup> and Huygens surfaces.<sup>14,15</sup>

Because of its high refractive index and compatibility with CMOS processes, silicon is widely used in all-dielectric metasurface devices, such as flat lenses,<sup>16–18</sup> achromatic lenses,<sup>19</sup> vortex generators,<sup>20,21</sup> holograms,<sup>22–25</sup> nonlinear

devices,<sup>26</sup> and metasurfaces controlled phase and polarization independently.<sup>27,28</sup> However, most of the silicon metasurface work is performed in the near-infrared wavelength regime and not in the visible. This is because most researchers use amorphous silicon (a-silicon) or polycrystalline silicon (poly-silicon) due to the ease of deposition onto transparent substrates such as glass. The problem with deposited silicon is its high absorption loss in the visible regime. Thin-film crystalline silicon (c-silicon) offers a solution to this problem because of its much lower absorption at  $\lambda > 500$  nm.<sup>29,30</sup> For example, the single-pass absorption of a 200 nm thin film of c-silicon and a-silicon is around 15% and 51% at a wavelength of 500 nm, respectively. The corresponding refractive index and extinction coefficient of c-silicon and a-silicon are  $n_{c-si} = 4.295$ ,  $k_{c-si} = 0.0719$ <sup>29</sup> and  $n_{a-si} = 4.497$ ,  $k_{a-si} = 0.45526$ .<sup>11</sup> While most researchers are aware that the absorption of c-silicon is lower

**Received:** September 28, 2016

**Published:** January 31, 2017



than that of a-silicon, it is not at all obvious that this difference is sufficient to enable the successful demonstration of high-efficiency metasurfaces in the visible regime. Metasurfaces must create large phase delay in order to operate efficiently, and the large phase delays are typically achieved with large aspect ratio nanostructures. In the case of high refractive index absorbing materials such as silicon, the question arises whether a sufficient phase delay can be achieved in a given thickness of material without excessive absorption. Since the phase delay and absorption are a function of the entire nanostructure and not the thin film alone, this question can be answered only by considering the structure as a whole. Alternatively, titanium dioxide (TiO<sub>2</sub>),<sup>31–33</sup> silicon nitride (Si<sub>3</sub>N<sub>4</sub>),<sup>34</sup> and silica (SiO<sub>2</sub>)<sup>35</sup> have been used for all-dielectric metasurfaces based on their high transparency throughout the visible spectrum. For example, a 600 nm thin TiO<sub>2</sub> film has recently been patterned into nanofins and posts in order to form a high numerical aperture (NA) metalens for operation at visible wavelengths.<sup>32,33</sup> Due to the lower refractive index contrast compared to silicon, however, these TiO<sub>2</sub> nanofins and posts require very high aspect ratios of 10–15<sup>32</sup> and 6,<sup>33</sup> respectively, which makes the fabrication very challenging.

Here, we propose the use of thin-film c-silicon as a metasurface material for visible light operation and demonstrate high efficiency polarization-independent operation in transmission at 532 nm wavelength. This demonstration is enabled by our layer-transfer technique, whereby we transfer 220 and 250 nm c-silicon device layers from a silicon on insulator (SOI) wafer to a transparent quartz substrate. The maximum aspect ratio of our metasurfaces is 3.4 in the experiment, which makes it easier to fabricate than comparable devices based on Si<sub>3</sub>N<sub>4</sub> or TiO<sub>2</sub>. We believe that this method will open a new way to extend the functionalities of metasurfaces efficiently into the visible light regime.

To illustrate the capability of our c-silicon metasurface in transmission and its full  $2\pi$  phase control, we consider light propagating through an array of circular c-silicon posts on a subwavelength square lattice (Figure 1).<sup>16,27</sup> Each post acts as a Fabry–Pérot resonator, and different diameter posts support modes of different effective index. Due to the circular symmetry of the circular posts, our metasurfaces are polarization-independent.

We performed the numerical calculation using the rigorous coupled-wave analysis (RCWA) method<sup>36</sup> and analyzed the transmission coefficient and phase of the periodic c-silicon posts by varying the unit cell size  $a$  from 160 to 250 nm and the diameter from  $0.2a$  to  $0.8a$  at the wavelength 532 nm (Figure 2a,b). In the calculation, the post height  $h$  is fixed to be 220 nm (refractive index from ref 29), the thickness of the silica film (refractive index  $n_{\text{Silica}} = 1.45$ ) and the adhesive NOA61 (Norland Products, Inc.) ( $n_{\text{NOA}} = 1.56$ ) underneath are 1  $\mu\text{m}$ , and the refractive index of the quartz substrate is 1.45. As shown in Figure 2, arrays of posts with 190 nm unit cell size can achieve large transmission amplitudes while spanning the full range of phases from 0 to  $2\pi$  by varying the diameter of the posts from 38 to 152 nm. In Table 1, which is based on Figure 2c, we choose eight different diameter posts with  $\pi/4$  increments to cover the full 0 to  $2\pi$  phase range.

To validate the phase control effect of our c-silicon metasurfaces, we designed a prism-like refractive index gradient as a beam deflector using the eight phase elements shown in Table 1. The diffraction angle  $\theta_t$  of such a gradient surface can be calculated via the generalized Snell's law,<sup>8</sup>

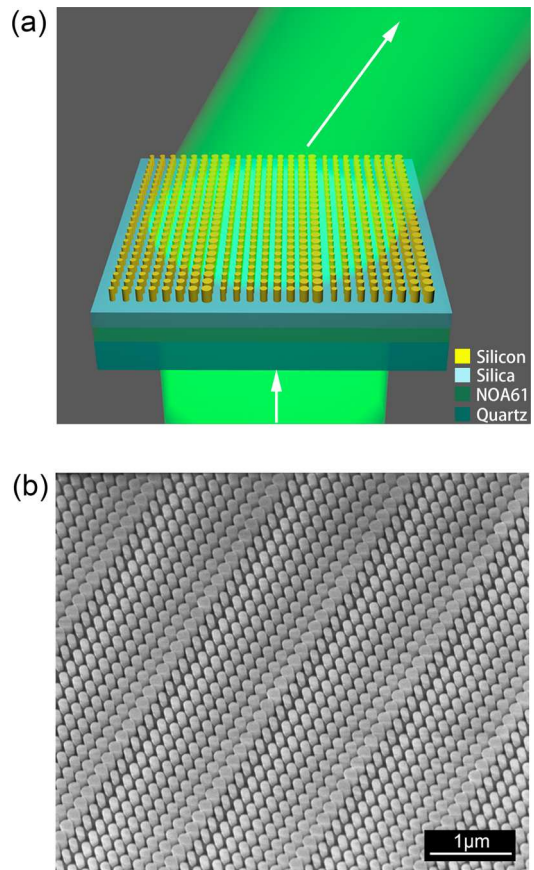


**Figure 1.** (a) Schematic of a gradient metasurface that acts as a beam deflector and (b) an SEM micrograph of our metasurface structure.

$$n_t \sin \theta_t - n_i \sin \theta_i = \frac{\lambda}{2\pi} \frac{d\Phi}{dx} \quad (1)$$

where  $n_t$  and  $n_i$  are the refractive index of the surrounding medium on the transmitted and incident sides,  $\theta_i$  is the incident light angle,  $\lambda$  is the vacuum wavelength, and  $d\Phi/dx$  is the phase gradient. In our case,  $d\Phi$  equals  $\pi/4$  and  $dx$  equals the unit cell size of 190 nm. Hence we expect that the gradient metasurfaces will deflect the transmitted beam at an angle of  $20.48^\circ$  to normal incidence.

We first performed an finite-difference time-domain (FDTD) simulation of the gradient metasurfaces. We observe that the light excites Fabry–Pérot-type resonances in each post (Figure 3a). As shown in Figure 3b, the diffraction angle observed from the phase profile is  $20.48^\circ$ . The same angle can also be calculated from Figure 3c by<sup>37</sup>

$$\theta = \sin^{-1}(k_x/k_0) = \sin^{-1}(0.35) = 20.48^\circ \quad (2)$$

Further, we obtain a transmission efficiency of 61% at 532 nm and an efficiency for the diffraction into the desired order of 97%. Here, these transmission and diffraction efficiencies are defined as<sup>11,17</sup>

$$\eta_T = I_{\text{out}}/I_{\text{input}} \quad (3)$$

$$\eta_{\text{diff}} = I_{1\text{rd}}/I_{\text{out}} \quad (4)$$

where  $I_{\text{input}}$  is the transmission intensity of the quartz substrate and  $I_{\text{out}}$  and  $I_{1\text{rd}}$  are the total transmission intensity and the +1 order diffraction intensity in transmission of the metasurfaces, respectively. We also define the deflection efficiency as

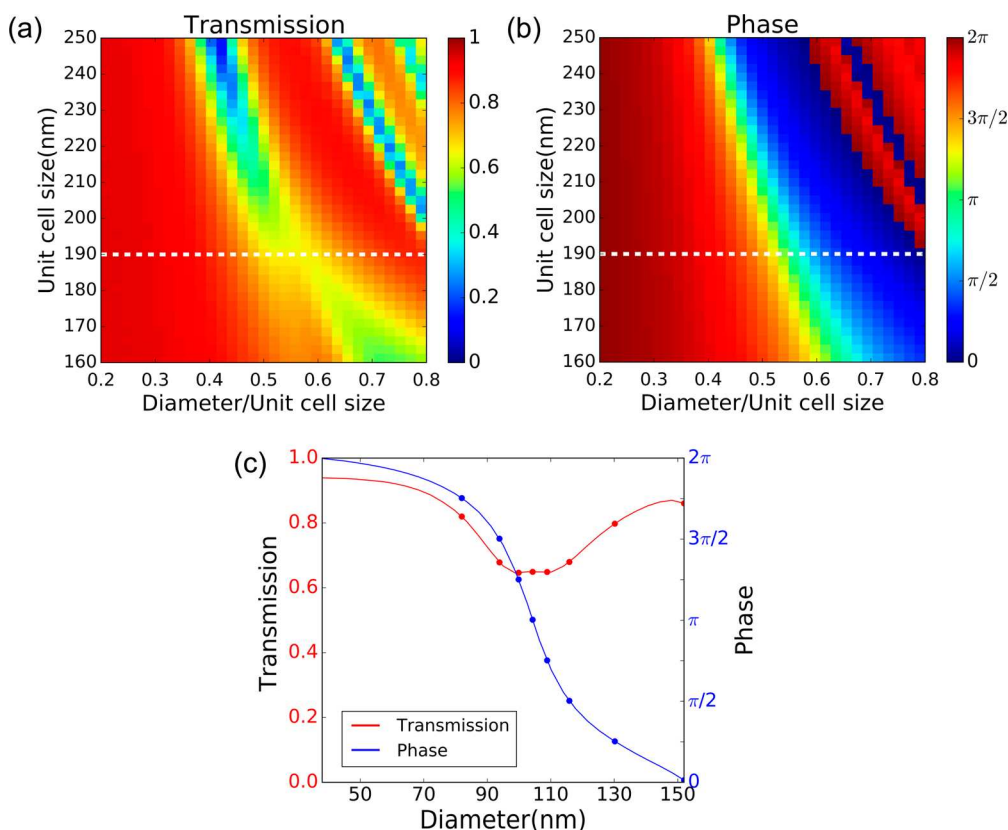


**Figure 2.** Calculation of (a) the transmission and (b) the phase of the periodic c-silicon posts on a square lattice with different unit cell size and diameters. (c) Transmission and phase of the periodic c-silicon posts with 190 nm unit cell size and 220 nm height for different diameters.

**Table 1. Diameters of Posts with 190 nm Unit Cell Size and 220 nm Height Required to Achieve Full  $2\pi$  Coverage in  $\pi/4$  Steps**

|               | phase (rad) |         |         |          |       |          |          |          |
|---------------|-------------|---------|---------|----------|-------|----------|----------|----------|
|               | 0           | $\pi/4$ | $\pi/2$ | $3\pi/4$ | $\pi$ | $5\pi/4$ | $3\pi/2$ | $7\pi/4$ |
| diameter (nm) | 152         | 130     | 116     | 109      | 104   | 100      | 94       | 82       |

$$\eta = I_{\text{rd}}/I_{\text{input}} \quad (5)$$

being equal to the product of diffraction efficiency and transmission efficiency into the desired diffraction order.

The difference between unity and the observed deflection efficiencies (59%) is mainly caused by the absorption of c-silicon (30%), interface reflectivity (8%), and other diffraction orders (3%). For the 220 nm film used here, the aspect ratio of the fabricated device is 2.7. As shown in Figure 4a, we have calculated the transmission efficiency and diffraction efficiency as a function of c-silicon thickness. For thin c-silicon, it is difficult to achieve full  $2\pi$  phase control for high diffraction efficiency and transmission, while for thicker c-silicon, the aspect ratio is too high, leading to high absorption and fabrication complexity. It is interesting to note that if we were to use a slightly thicker film of 250 nm and a 3.4 aspect ratio, we could increase the transmission further to 73% (Figure 4b,c) even though the silicon is an absorbing material at that wavelength. Furthermore, the value is close to the result of 78% obtained with polarization-independent metasurfaces by  $\text{TiO}_2$ <sup>31</sup> and which requires a much higher aspect ratio and hence more demanding fabrication.

We also simulated the full-width at half-maximum (fwhm) of the diffraction efficiency for both the 220 and 250 nm metasurfaces made in c-silicon and a-silicon in Figure S3 of the Supporting Information. We obtain bandwidths around 100 and 65 nm fwhm for the c-silicon and the a-silicon metasurfaces, respectively.

Thin-film c-silicon from an SOI wafer can be transferred to a rigid or a flexible substrate using a lift-off and stamp printing process<sup>38,39</sup> or by adhesive wafer bonding and deep reactive ion etching (DRIE).<sup>40,41</sup> We used the latter method because we found it easier to maintain the integrity of the nanostructure. We then used electron beam lithography (EBL) to define the pattern. Our fabrication process is illustrated in Figure 5.

First, we deposit 1  $\mu\text{m}$  silica on a SOITEC SOI wafer comprising a 220 or 250 nm thin-film c-silicon layer on 2  $\mu\text{m}$  of silica. This 1  $\mu\text{m}$  silica layer protects the c-silicon from the adhesives and quartz (Figure 5a). Next, we spin the UV curable adhesive NOA61 on the sample followed by bonding to the quartz substrate (Figure 5b and c). Then the sample is illuminated by 365 nm ultraviolet LED light to cross-link the NOA61 polymer for 2 h. In order to obtain optimum adhesion, the sample is baked at 50  $^{\circ}\text{C}$  for 2 days (Figure 5d). The silicon substrate is then removed by first milling down to near 40  $\mu\text{m}$  followed by DRIE (Figure 5e). Finally, the c-silicon on quartz substrate is obtained by removing the silica of the SOI wafer using HF acid.

The fabrication process of the metasurfaces on the c-silicon by EBL is shown in Figure 5g–i. The sample is spin-coated with 180 nm ZEP520A electron beam resist followed by a 50 nm aluminum layer (thermal evaporation) to serve as the charge dissipation layer. The pattern is then exposed using a



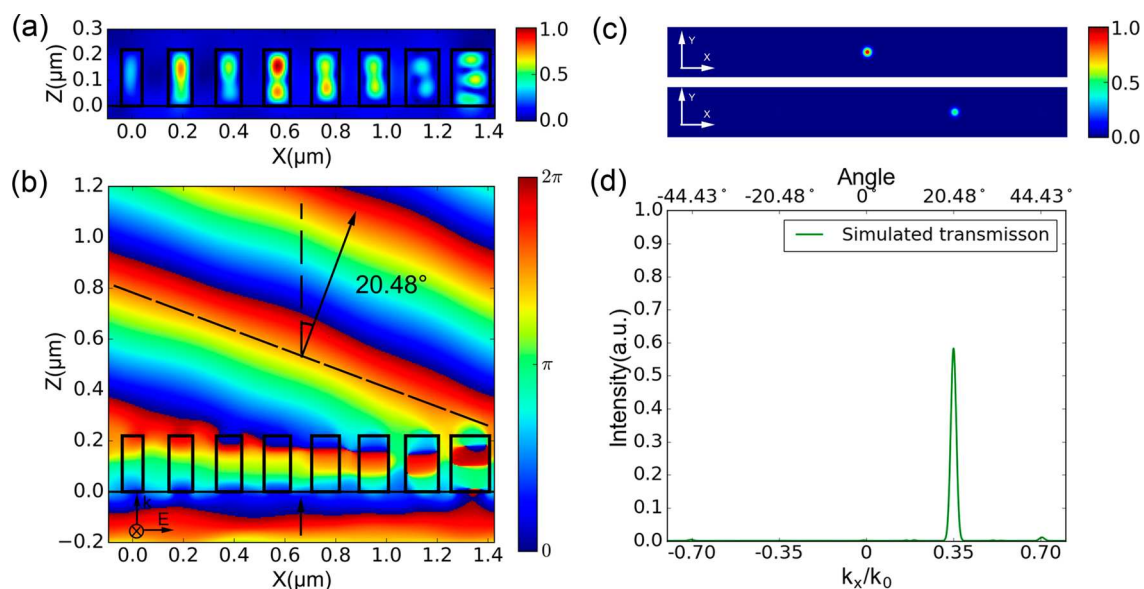


**Figure 3.** FDTD simulation of the gradient metasurface. (a) Mode profile for each 220 nm thick c-silicon post of the deflector, showing the magnetic field amplitude in the  $xz$  plane ( $H_{xz}$ ) for a wavelength of 532 nm. We start with the smallest post on the left and gradually increase the size toward the largest post on the right. (b) Phase profile obtained by the metasurface resulting in a diffraction angle of  $20.48^\circ$ . (c) Far-field profiles of the incident light intensity (top) and transmission intensity (bottom). (d) Transmitted deflected beam intensity normalized to the input signal in the  $k_x$  direction.

194 Raith Vistec EBPG-5000plusES electron beam writer at 100  
195 keV. After exposure, the aluminum layer is removed by  
196 tetramethylammonium hydroxide and the resist is developed  
197 with xylene. Then the pattern transfer is etched using an  
198 Oxford Instruments inductively coupled plasma tool.

199 The overall area of the fabricated gradient metasurface is 200  
200  $\mu\text{m} \times 200 \mu\text{m}$ . As shown in Figure 6a, we used a 532 nm cw  
201 laser for illumination, linear polarizers, and a half-wave plate to  
202 change the polarization direction of the input light. A 4 $\times$   
203 objective (Obj1, 0.1 NA) was used to focus the light onto the  
204 sample with a spot diameter of  $\sim 150 \mu\text{m}$ . A 100 $\times$  objective  
205 (Obj2, 0.9 NA) was used to collect the transmitted signal. The  
206 real-space and  $k$ -space (diffraction order) image of the sample  
207 was captured by the CCD, respectively (Figure 6a). From  
208 Figure 6b and c, we can see that the metasurface directs the  
209 light almost entirely into the +1 order, while the other  
210 diffraction orders are too weak to be captured by the CCD. The  
211 diffraction angle is measured to be  $21^\circ$ , which is close to the  
212 theoretical calculation and the numerical simulation. For the  
213 220 nm thin film c-silicon design, the transmission efficiency  
214 and the diffraction efficiency are measured to be 51% and 93%  
215 by using the intensity value measured by the optical power  
216 meter. As predicted by theory, the measured transmission  
217 efficiency was polarization-independent with only 5% variation  
218 (Figure 6d). This small variation may come not only from  
219 fabrication imperfections but also from cross-talk between  
220 different meta-atoms in the array.<sup>25</sup> For the 250 nm thin film c-  
221 silicon design, the transmission efficiency and the diffraction  
222 efficiency can be improved to be 71% and 95% in the  
223 experiment (Figure 6e).

224 It is known that the transmission efficiency of plasmonic  
225 metasurfaces is limited to 25%<sup>16</sup> because of ohmic loss, which is  
226 absent in dielectric metasurfaces. In order to highlight the  
227 improvement achieved with different types of dielectric  
228 metasurfaces, we compare the experimental transmission in  
229 the near-infrared and the visible regime in Table 2. The  
230 deflection efficiency is defined as above (eq 5), being equal to

the product of diffraction efficiency and transmission efficiency. 231  
The aspect ratio is defined as the ratio of the minimum feature 232  
size of the nanostructure to the thickness of the material. 233

As shown in Table 2, low-index-contrast metasurfaces such as 234  
quartz<sup>35</sup> and  $\text{TiO}_2$ <sup>31</sup> offer higher transmission in the visible 235  
regime, but they also require higher thickness and very high 236  
aspect ratios to achieve a full 0 to  $2\pi$  phase range for 237  
polarization-independent operation. For example, the quartz 238  
structure requires an aspect ratio of 10 for 633 nm operation, 239  
which makes it difficult to fabricate precisely. Poly-silicon and a-  
silicon metasurfaces can be fabricated much more easily due to 240  
their higher refractive index and lower aspect ratios. But the 241  
deflection efficiency is limited in the shorter wavelength range 242  
because of absorption loss, and reported efficiencies are below 243  
30% at 500 nm even for polarization-dependent designs.<sup>17</sup> By 244  
improving the structure, Yu et al.<sup>11</sup> demonstrated a 45% 245  
deflection efficiency at 705 nm in a-silicon, but were not able to 246  
obtain high efficiency at 500 nm, which is very important for 247  
display applications. By comparison, c-silicon metasurfaces offer 248  
significant advantages compared to these materials. Metasur- 249  
faces based on c-Si operate with a thinner film and a lower aspect 250  
ratio than  $\text{TiO}_2$ , and they achieve better transmission than poly- 251  
silicon and a-silicon in the visible regime. On the basis of a 252  
simple transfer technique, the c-silicon can be easily transferred 253  
to the desired substrate from an SOI wafer. Due to its high 254  
refractive index, the c-silicon pattern can be easily fabricated 255  
and surrounded with other low-index materials to increase the 256  
numerical aperture of metalenses and flexible metasurfaces.<sup>37,42</sup> 257  
258

Having now experimentally demonstrated a deflection 259  
efficiency of 47%, let us consider further improvements. First 260  
of all, we note a discrepancy of 12% between the simulated 261  
efficiency (59%, Figure 3c) and the experimental value. This 262  
discrepancy can be explained by fabrication tolerances; by 263  
analyzing the as-fabricated structures, we note an average size 264  
discrepancy in pillar diameter of 7 nm. If we use this adjusted 265  
size in our simulation, the calculated efficiency becomes 45%, 266  
i.e., similar to the experimental value within measurement error. 267

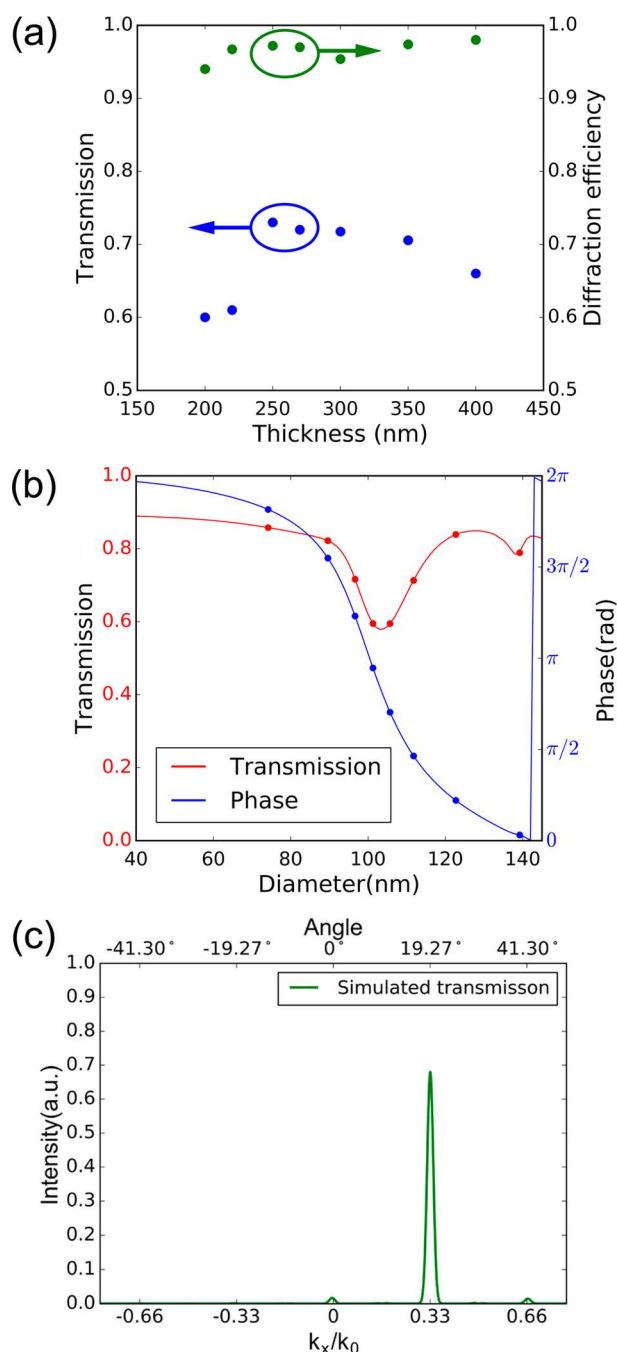


**Figure 4.** Calculation of (a) the transmission efficiency and diffraction efficiency of the deflectors as a function of c-silicon thickness. The corresponding metasurface designs are shown in Table S1. (b) Transmission and phase of the periodic c-silicon posts with 200 nm unit cell size for 250 nm film thickness. (c) FDTD simulation of the transmitted beam intensity normalized to the input signal in the  $k_x$  direction for the 250 nm thick film.

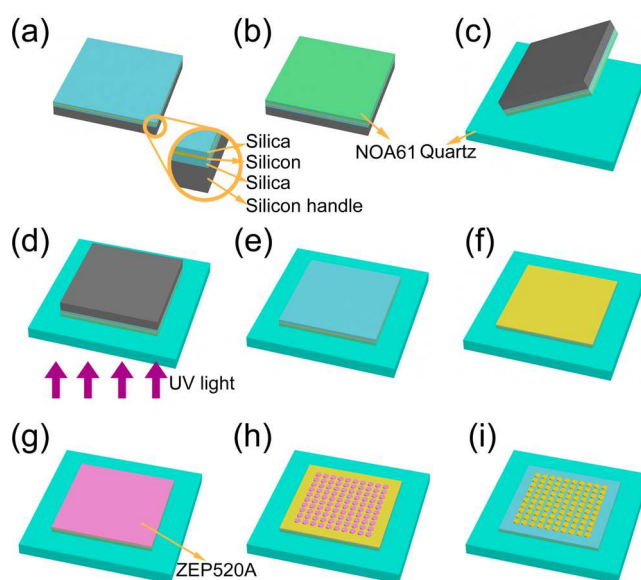


**Figure 5.** Schematic illustration of the c-silicon transfer process and sample fabrication. (a) Deposition of silica on an SOI wafer using ICP-CVD. (b) Spin-coating adhesive NOA61 (c) Bonding SOI with fused quartz. (d) Exposing with UV light for 2 h, followed by baking for 2 days at 50 °C. (e) Polishing the silicon substrate to ~40 μm, then removing the remaining silicon substrate by DRIE. (f) Removing the silica layer with HF acid. (g) Spinning ZEP520A and depositing Al. (h) Exposing the pattern by EBL and removing Al. (i) Transferring the pattern to silicon by ICP, then removing the resist by 1165 remover and O<sub>2</sub> plasma ashing.

to 250 nm allows us to push the efficiency even further, i.e., up to 71% in simulation (Figure 4b) and 67% in experiment (Figure 6e). Demonstrating the possibility of achieving such a high efficiency for visible light with silicon is a truly surprising outcome of this work. We verify that diameter variations are indeed responsible for the discrepancy between simulation and experiment, as the variations are smaller for the 250 nm sample and, correspondingly, the discrepancy is smaller as well.

In summary, we have transferred thin-film c-silicon onto a quartz substrate by adhesive wafer bonding, then demonstrated c-silicon gradient metasurfaces for beam deflection at a wavelength of 532 nm. Furthermore, our experiment demonstrates full  $2\pi$  phase control. We demonstrate a polarization-independent transmission efficiency of 71% with 95% diffraction efficiency. The corresponding deflection efficiency is 67%, and our simulations show that it can be increased up to 71%, which is very close to the values achieved with TiO<sub>2</sub>, yet with a lower aspect ratio, hence reduced fabrication complexity, if we use commercially available silicon on glass samples.<sup>44,45</sup> This lower aspect ratio also achieved high phase delay while reducing the absorption and fabrication complexity, which make it possible to achieve high efficiency metasurfaces comparable with TiO<sub>2</sub>.

We believe that this approach not only can be applied to other wavefront shaping situations, such as focusing, vortex generation, and holography, but also offers a viable route to efficient tunable metasurfaces on flexible substrates in the visible range. Our geometry is also attractive for a variety of applications in integrated optics, such as imaging, biomedical sciences, or wearable consumer electronics.

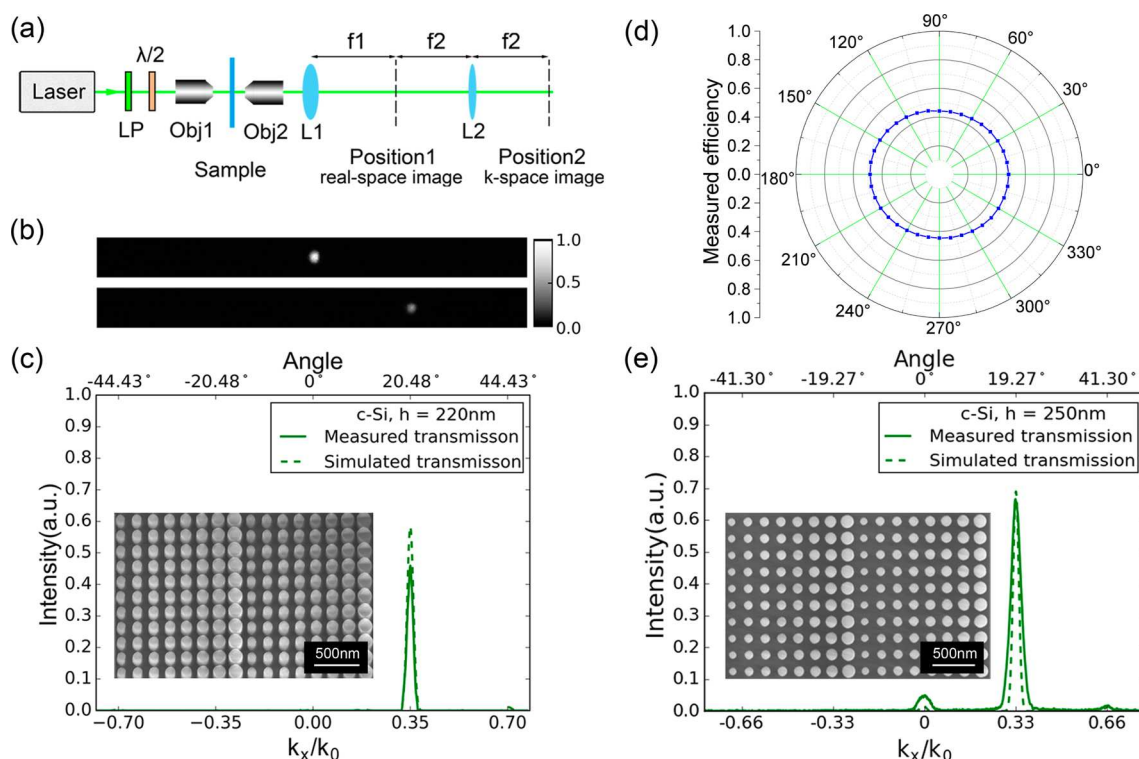


**Figure 6.** (a) Measurement setup used to characterize the metasurfaces according to the design shown in Table 1. (b) Far-field profiles of the incident light intensity (top) and transmitted intensity (bottom) captured by a CCD camera. (c) Experiment (solid line, calculated from the CCD camera data in panel b) and simulation (dashed line, same as Figure 3c) of the transmitted deflected beam intensity normalized to the input signal in the  $k_x$  direction of the 220 nm thin film c-silicon design. The inset shows an SEM micrograph of the structure. (d) Measured transmission efficiency with different polarization directions of the 220 nm thin film c-silicon design. The polarization direction is defined as the angle between the electric field and gradient of the posts. (e) Experiment and simulation of the transmitted deflected beam intensity of the 250 nm thin film c-silicon design.

**Table 2. Summary of Previously Reported Experimental Metasurfaces Used as Deflectors Operating in Transmission in the Visible Range**

| ref                           | material         | wavelength | deflection efficiency | polarization | building block | thickness          | aspect ratio |
|-------------------------------|------------------|------------|-----------------------|--------------|----------------|--------------------|--------------|
| Chen et al. <sup>35</sup>     | quartz           | 633 nm     | 55%                   | independence | square posts   | 1.38 $\mu\text{m}$ | 10           |
| Astilean et al. <sup>43</sup> | TiO <sub>2</sub> | 633 nm     | 85%                   | linear       | 1D grating     | 540 nm             | 5.3          |
| Lalanne et al. <sup>31</sup>  | TiO <sub>2</sub> | 633 nm     | 78%                   | independence | square posts   | 487 nm             | 4.6          |
| Yu et al. <sup>11</sup>       | a-silicon        | 705 nm     | 45%                   | independence | circular posts | 130 nm             | 0.93         |
| Lin et al. <sup>17</sup>      | p-silicon        | 500 nm     | 29%                   | circular     | nanobeams      | 100 nm             | 1.2          |
| this work (experiment)        | c-silicon        | 532 nm     | 47%                   | independence | circular posts | 220 nm             | 2.47         |
| this work (simulation)        | c-silicon        | 532 nm     | 59%                   | independence | circular posts | 220 nm             | 2.7          |
| this work (experiment)        | c-silicon        | 532 nm     | 67%                   | independence | circular posts | 250 nm             | 3.4          |
| this work (simulation)        | c-silicon        | 532 nm     | 71%                   | independence | circular posts | 250 nm             | 3.4          |

## ASSOCIATED CONTENT

### Supporting Information

The Supporting Information is available free of charge on the ACS Publications website at DOI: 10.1021/acsphotonics.6b00740.

Simulation of the deflecting achieved by our metasurfaces for c-silicon and a-silicon; the parameter and bandwidth of our designed metasurfaces. (PDF)

## AUTHOR INFORMATION

### Corresponding Author

\*E-mail: wangxueh@mail.sysu.edu.cn.

### ORCID

Zhenpeng Zhou: 0000-0001-9712-0866

### Author Contributions

<sup>||</sup>Z. Zhou and J. Li contributed equally to this work.

### Notes

The authors declare no competing financial interest.

## ACKNOWLEDGMENTS

This work is supported by Ministry of Science and Technology of China (2016YFA0301300), National Natural Science Foundation of China (11674402, 11334015, 11304102), Guangzhou Science and Technology Projects (201607010044, 201607020023), Natural Science Foundation of Guangdong (2016A030312012), the Fundamental Research Funds for the Central Universities, the Open Research Project of the State Key Laboratory of Optoelectronic Materials and Technologies in Sun Yat-Sen University of China, and EPSRC of U.K. under Grant EP/J01771X/1 (Structured Light). We



335 also would like to acknowledge Prof. Jianwen Dong for useful  
336 discussions on the metasurface design.

## 337 ■ REFERENCES

- 338 (1) Zheludev, N. I.; Kivshar, Y. S. From metamaterials to  
339 metadevices. *Nat. Mater.* **2012**, *11*, 917–924.
- 340 (2) Meinzer, N.; Barnes, W. L.; Hooper, I. R. Plasmonic meta-atoms  
341 and metasurfaces. *Nat. Photonics* **2014**, *8*, 889–898.
- 342 (3) Yu, N.; Capasso, F. Flat optics with designer metasurfaces. *Nat.*  
343 *Mater.* **2014**, *13*, 139–150.
- 344 (4) Minovich, A. E.; Miroshnichenko, A. E.; Bykov, A. Y.; Murzina, T.  
345 V.; Neshev, D. N.; Kivshar, Y. S. Functional and nonlinear optical  
346 metasurfaces. *Laser Photonics Rev.* **2015**, *9*, 195–213.
- 347 (5) Glybovski, S. B.; Tretyakov, S. A.; Belov, P. A.; Kivshar, Y. S.;  
348 Simovski, C. R. Metasurfaces: From microwaves to visible. *Phys. Rep.*  
349 **2016**, *634*, 1–72.
- 350 (6) Wan, C.; Ho, Y.; Nunez-Sanchez, S.; Chen, L.; Lopez-Garcia, M.;  
351 Pugh, J.; Zhu, B.; Selvaraj, P.; Mallick, T.; Senthilarasu, S.; Cryan, M. J.  
352 A selective metasurface absorber with an amorphous carbon interlayer  
353 for solar thermal applications. *Nano Energy* **2016**, *26*, 392–397.
- 354 (7) West, P. R.; Ishii, S.; Naik, G. V.; Emani, N. K.; Shalae, V. M.;  
355 Boltasseva, A. Searching for better plasmonic materials. *Laser Photonics*  
356 *Rev.* **2010**, *4*, 795–808.
- 357 (8) Yu, N.; Genevet, P.; Kats, M. A.; Aieta, F.; Tetienne, J. P.;  
358 Capasso, F.; Gaburro, Z. Light propagation with phase discontinuities:  
359 generalized laws of reflection and refraction. *Science* **2011**, *334*, 333–  
360 337.
- 361 (9) Fattal, D.; Li, J.; Peng, Z.; Fiorentino, M.; Beausoleil, R. G. Flat  
362 dielectric grating reflectors with focusing abilities. *Nat. Photonics* **2010**,  
363 *4*, 466–470.
- 364 (10) Jahani, S.; Jacob, Z. All-dielectric metamaterials. *Nat. Nano-*  
365 *technol.* **2016**, *11*, 23–36.
- 366 (11) Yu, Y. F.; Zhu, A. Y.; Paniagua-Domínguez, R.; Fu, Y. H.;  
367 Luk'yanchuk, B.; Kuznetsov, A. I. High-transmission dielectric  
368 metasurface with  $2\pi$  phase control at visible wavelengths. *Laser*  
369 *Photonics Rev.* **2015**, *9*, 412–418.
- 370 (12) Moitra, P.; Slovick, B. A.; Gang, Y. Z.; Krishnamurthy, S.;  
371 Valentine, J. Experimental demonstration of a broadband all-dielectric  
372 metamaterial perfect reflector. *Appl. Phys. Lett.* **2014**, *104*, 171102.
- 373 (13) Esfandyarpour, M.; Garnett, E. C.; Cui, Y.; McGehee, M. D.;  
374 Brongersma, M. L. Metamaterial mirrors in optoelectronic devices.  
375 *Nat. Nanotechnol.* **2014**, *9*, 542–547.
- 376 (14) Staude, I.; Miroshnichenko, A. E.; Decker, M.; Fofang, N. T.;  
377 Liu, S.; Gonzales, E.; Dominguez, J.; Luk, T. S.; Neshev, D. N.; Brener,  
378 I.; Kivshar, Y. Tailoring directional scattering through magnetic and  
379 electric resonances in subwavelength silicon nanodisks. *ACS Nano*  
380 **2013**, *7*, 7824–7832.
- 381 (15) Decker, M.; Staude, I.; Falkner, M.; Dominguez, J.; Neshev, D.  
382 N.; Brener, I.; Pertsch, T.; Kivshar, Y. S. High-Efficiency Dielectric  
383 Huygens' Surfaces. *Adv. Opt. Mater.* **2015**, *3*, 813–820.
- 384 (16) Arbabi, A.; Horie, Y.; Ball, A. J.; Bagheri, M.; Faraon, A.  
385 Subwavelength-thick lenses with high numerical apertures and large  
386 efficiency based on high-contrast transmitarrays. *Nat. Commun.* **2015**,  
387 *6*, 7069.
- 388 (17) Lin, D.; Fan, P.; Hasman, E.; Brongersma, M. L. Dielectric  
389 gradient metasurface optical elements. *Science* **2014**, *345*, 298–302.
- 390 (18) Klemm, A. B.; Stellinga, D.; Martins, E. R.; Lewis, L.; Huyet, G.;  
391 O'Faolain, L.; Krauss, T. F. Experimental high numerical aperture  
392 focusing with high contrast gratings. *Opt. Lett.* **2013**, *38*, 3410–3413.
- 393 (19) Aieta, F.; Kats, M. A.; Genevet, P.; Capasso, F. Applied optics.  
394 Multiwavelength achromatic metasurfaces by dispersive phase  
395 compensation. *Science* **2015**, *347*, 1342–1345.
- 396 (20) Chong, K. E.; Staude, I.; James, A.; Dominguez, J.; Liu, S.;  
397 Campione, S.; Subramania, G. S.; Luk, T. S.; Decker, M.; Neshev, D.  
398 N.; Brener, I.; Kivshar, Y. S. Polarization-Independent Silicon  
399 Metadevices for Efficient Optical Wavefront Control. *Nano Lett.*  
400 **2015**, *15*, 5369–5374.
- 401 (21) Shalae, M. I.; Sun, J.; Tsukernik, A.; Pandey, A.; Nikolskiy, K.;  
402 Litchinitser, N. M. High-Efficiency All-Dielectric Metasurfaces for

- 403 Ultracompact Beam Manipulation in Transmission Mode. *Nano Lett.* **2015**, *15*, 6261–6266.
- 404 (22) Khorasaninejad, M.; Ambrosio, A.; Kanhaiya, P.; Capasso, F.  
405 Broadband and chiral binary dielectric meta-holograms. *Sci. Adv.* **2016**,  
406 *2*, e1501258.
- 407 (23) Wang, B.; Dong, F.; Li, Q. T.; Yang, D.; Sun, C.; Chen, J.; Song,  
408 Z.; Xu, L.; Chu, W.; Xiao, Y. F.; Gong, Q.; Li, Y. Visible-Frequency  
409 Dielectric Metasurfaces for Multiwavelength Achromatic and Highly  
410 Dispersive Holograms. *Nano Lett.* **2016**, *16*, 5235–5240.
- 411 (24) Chong, K. E.; Wang, L.; Staude, I.; James, A. R.; Dominguez, J.;  
412 Liu, S.; Subramania, G. S.; Decker, M.; Neshev, D. N.; Brener, I.;  
413 Kivshar, Y. S. Efficient Polarization-Insensitive Complex Wavefront  
414 Control Using Huygens' Metasurfaces Based on Dielectric Resonant  
415 Meta-atoms. *ACS Photonics* **2016**, *3*, 514–519.
- 416 (25) Li, Q.-T.; Wang, B.; Gan, F.; Chen, J.; Song, Z.; Xu, L.; Chu, W.;  
417 Xiao, Y.-F.; Gong, Q.; Li, Y. Polarization-independent and  
418 high-efficiency dielectric metasurfaces for visible light. *Opt. Express*  
419 **2016**, *24*, 16309.
- 420 (26) Yang, Y.; Wang, W.; Boulesbaa, A.; Kravchenko, I.; Briggs, D.  
421 P.; Poretzky, A.; Geohegan, D.; Valentine, J. Nonlinear Fano-Resonant  
422 Dielectric Metasurfaces. *Nano Lett.* **2015**, *15*, 7388–7393.
- 423 (27) Arbabi, A.; Horie, Y.; Bagheri, M.; Faraon, A. Dielectric  
424 metasurfaces for complete control of phase and polarization with  
425 subwavelength spatial resolution and high transmission. *Nat. Nano-*  
426 *technol.* **2015**, *10*, 937–943.
- 427 (28) Backlund, M. P.; Arbabi, A.; Petrov, P. N.; Arbabi, E.; Saurabh,  
428 S.; Faraon, A.; Moerner, W. E. Removing Orientation-Induced  
429 Localization Biases in Single-Molecule Microscopy Using a Broadband  
430 Metasurface Mask. *Nat. Photonics* **2016**, *10*, 459–462.
- 431 (29) Palik, E. D. *Handbook of Optical Constants of Solids*; Academic  
432 Press: San Diego, 1985.
- 433 (30) Evlyukhin, A. B.; Novikov, S. M.; Zywietz, U.; Eriksen, R. L.;  
434 Reinhardt, C.; Bozhevolnyi, S. I.; Chichkov, B. N. Demonstration of  
435 magnetic dipole resonances of dielectric nanospheres in the visible  
436 region. *Nano Lett.* **2012**, *12*, 3749–3755.
- 437 (31) Lallanne, P.; Astilean, S.; Chavel, P.; Cambil, E.; Launois, H.  
438 Blazed binary subwavelength gratings with efficiencies larger than  
439 those of conventional échelle gratings. *Opt. Lett.* **1998**, *23*, 1081.
- 440 (32) Khorasaninejad, M.; Chen, W. T.; Devlin, R. C.; Oh, J.; Zhu, A.  
441 Y.; Capasso, F. Metalenses at visible wavelengths: Diffraction-limited  
442 focusing and subwavelength resolution imaging. *Science* **2016**, *352*,  
443 1190–1194.
- 444 (33) Khorasaninejad, M.; Zhu, A. Y.; Roques-Carmes, C.; Chen, W.  
445 T.; Oh, J.; Mishra, I.; Devlin, R. C.; Capasso, F. Polarization-  
446 Insensitive Metalenses at Visible Wavelengths. *Nano Lett.* **2016**, *16*,  
447 7229–7234.
- 448 (34) Zhan, A.; Colburn, S.; Trivedi, R.; Fryett, T. K.; Dodson, C. M.;  
449 Majumdar, A. Low-Contrast Dielectric Metasurface Optics. *ACS*  
450 *Photonics* **2016**, *3*, 209–214.
- 451 (35) Chen, F. T.; Craighead, H. G. Diffractive phase elements based  
452 on two-dimensional artificial dielectrics. *Opt. Lett.* **1995**, *20*, 121–123.
- 453 (36) Li, L. New formulation of the Fourier modal method for crossed  
454 surface-relief gratings. *J. Opt. Soc. Am. A* **1997**, *14*, 2758.
- 455 (37) Ee, H. S.; Agarwal, R. Tunable Metasurface and Flat Optical  
456 Zoom Lens on a Stretchable Substrate. *Nano Lett.* **2016**, *16*, 2818–  
457 2823.
- 458 (38) Meitl, M. A.; Zhu, Z.-T.; Kumar, V.; Lee, K. J.; Feng, X.; Huang,  
459 Y. Y.; Adesida, I.; Nuzzo, R. G.; Rogers, J. A. Transfer printing by  
460 kinetic control of adhesion to an elastomeric stamp. *Nat. Mater.* **2006**,  
461 *5*, 33–38.
- 462 (39) Xu, X.; Subbaraman, H.; Hosseini, A.; Lin, C. Y.; Kwong, D.;  
463 Chen, R. T. Stamp printing of silicon-nanomembrane-based photonic  
464 devices onto flexible substrates with a suspended configuration. *Opt.*  
465 *Lett.* **2012**, *37*, 1020–1022.
- 466 (40) Niklaus, F.; Stemme, G.; Lu, J. Q.; Gutmann, R. J. Adhesive  
467 wafer bonding. *J. Appl. Phys.* **2006**, *99*, 031101.
- 468 (41) Zablocki, M. J.; Sharkawy, A.; Ebil, O.; Prather, D. W.  
469 Nanomembrane transfer process for intricate photonic device  
470 applications. *Opt. Lett.* **2011**, *36*, 58–60.
- 471



- 472 (42) Zhu, L.; Kapraun, J.; Ferrara, J.; Chang-Hasnain, C. J. Flexible  
473 photonic metastructures for tunable coloration. *Optica* **2015**, *2*, 255.  
474 (43) Astilean, S.; Lalanne, P.; Chavel, P.; Cambril, E.; Launois, H.  
475 High-efficiency subwavelength diffractive element patterned in a high-  
476 refractive-index material for 633 nm. *Opt. Lett.* **1998**, *23*, 552–554.  
477 (44) Kim, H. S.; Blick, R. H.; Kim, D. M.; Eom, C. B. Bonding  
478 silicon-on-insulator to glass wafers for integrated bio-electronic  
479 circuits. *Appl. Phys. Lett.* **2004**, *85*, 2370–2372.  
480 (45) MEMS Engineering and Material Home Page. [http://www.](http://www.memsengineering.com)  
481 [memsengineering.com](http://www.memsengineering.com) (accessed January 30, 2017).<sup>1</sup>